Cell Proliferation

Cell Prolif., 2016, **49**, 134–144 doi: 10.1111/cpr.12234

Magnetic assembly of 3D cell clusters: visualizing the formation of an engineered tissue

S. Ghosh*, S. R. P. Kumar†, I. K. Puri*,‡ and S. Elankumaran†

**Department of Engineering Physics, McMaster University, Hamilton, ON, Canada, †Department of Biomedical Sciences and Pathobiology, Virginia-Maryland Regional College of Veterinary Medicine, Virginia Tech, Blacksburg, VA, USA and ‡Department of Mechanical Engineering, McMaster University, Hamilton, ON, Canada*

Received 24 July 2015; revision accepted 12 September 2015

Abstract

Objectives: Contactless magnetic assembly of cells into 3D clusters has been proposed as a novel means for 3D tissue culture that eliminates the need for artificial scaffolds. However, thus far its efficacy has only been studied by comparing expression levels of generic proteins. Here, it has been evaluated by visualizing the evolution of cell clusters assembled by magnetic forces, to examine their resemblance to *in vivo* tissues.

Materials and methods: Cells were labeled with magnetic nanoparticles, then assembled into 3D clusters using magnetic force. Scanning electron microscopy was used to image intercellular interactions and morphological features of the clusters.

Results: When cells were held together by magnetic forces for a single day, they formed intercellular contacts through extracellular fibers. These kept the clusters intact once the magnetic forces were removed, thus serving the primary function of scaffolds. The cells self-organized into constructs consistent with the corresponding tissues *in vivo*. Epithelial cells formed sheets while fibroblasts formed spheroids and exhibited position-dependent morphological heterogeneity. Cells on the periphery of a cluster were flattened while those within were spheroidal, a well-known characteristic of connective tissues *in vivo*.

Conclusions: Cells assembled by magnetic forces presented visual features representative of their *in vivo* states but largely absent in monolayers. This established the efficacy of contactless assembly as a means to fabricate *in vitro* tissue models.

Correspondence: Dr. Subbiah Elankumaran, Department of Biomedical Sciences and Pathobiology, Virginia Tech, 1981 Kraft Dr, Blacksburg, VA 24061, USA. Tel.: +1 540-231-0761; Fax: +1 540-231-3414. E-mail: kumarans@vt.edu

Introduction

Three-dimensional (3D) clusters of cells are able to mimic *in vivo* conditions better than monolayers (1–4). This is because features of cells, for example morphology and gene expression, are strongly influenced by their microenvironment - neighboring cells (5) and the extracellular matrix (ECM) (6). Popular 3D cell culture methods employ scaffolds to position cells in 3D architecture (7,8). A wide variety of artificial scaffolding materials is used, ranging from synthetic polymers (9,10) to extracellular proteins of animal origin (11). They enable cell-cell interactions encountered *in vivo*. However, cell behaviour is also strongly regulated by several aspects of the ECM, such as its mechanical stiffness, chemical composition and topography (12). Thus, tissue cultured in an artificial scaffold is often not a faithful representation of its *in vivo* form (11,13). One solution is to design scaffolds that closely mimic the *in vivo* ECM for each individual cell type (14). A more convenient route, however, is to eliminate the use of scaffolds altogether, and to assemble the cells into 3D clusters using a contactless means, such as gravity (4), centrifugation (15) or magnetophoresis (16,17). Cells thus assembled are known to generate their own ECM (18), thus eliminating the need for mechanical support from artificial scaffolds.

Contactless magnetic manipulation of cells has been explored for decades (19–22), serving a variety of applications, for example, cell-sorting (23), tissue engineering (24,25) and as novel experimental tools (16,26,27). Manipulation is achieved by labeling the cells with magnetic nanoparticles (MNPs) coated in cytocompatible materials (28–30). Thus magnetized, the cells can be organized into structures of desired shape and size, such as in clusters (27,31), spheroids (16,17,32), thick

sheets (33–36) and tubes (37–41), by *a priori* determining the required magnetic field (42–46). Further, prescribed heterogeneities in population constitution of the culture can be patterned (24,47). These features are crucial for sophisticated experiments, such as being able to understand influences of intercellular communications in tumourigenesis (48,49), but are not achievable with centrifugal or gravitational forces.

The last decade has seen several reports on magnetic assembly of cells for 3D tissue culture (50). However, all thus far have established their efficacy by observing expression levels of generic proteins, such as transmembrane adhesion proteins (E-cadherin and N-cadherins), cytoskeletal proteins (actin and vimentin) and ECM proteins (collagen and fibronectin) (16,17,51,52). Results have been compared to monolayers and established 3D tissue culture methods, such as xenografts, centrifugal pelleting or the hanging drop method. Protein content is a well-known measure of tissue function and forms a logical choice as a metric of efficacy. However, it is impossible to specify an exhaustive list of proteins that needs to be probed in order to conclude that a group of cells has transformed into a tissue. Such a list is also very specific to cell type. Thus, a universal test for evaluating efficacy of a tissue engineering method is as yet unknown.

Any method to 'assemble' cells into an artificial tissue must cause them to form contacts with their neighbours. Further, they must collectively organize into a construct that resembles the morphology of the corresponding tissue *in vivo* (1). These two observations form more universally applicable indicators of tissue formation than protein expression levels. However, reports examining these facets are unavailable in the current literature. Histological analyses using H&E staining (37,38,51) provide only limited understanding of tissue architecture, but do not inform on either intercellular contacts or tissue morphology. Here we present visual evidence of both in clusters of magnetically assembled cells using scanning electron microscopy (SEM). When the cells were held in close proximity for a day, they formed intercellular contacts facilitated by extracellular fibers. Through these, the cells underwent collective re-organization. Epithelial cells formed multi-layer sheets while fibroblasts formed spheroids. Thus, the shape of such clusters was consistent with the physical form of the corresponding tissues *in vivo*. Further, the fibroblasts in 3D clusters exhibited position- and possibly, function-dependent morphological heterogeneities; the cells on the periphery of the clusters assumed flattened skin-like forms while the cells within were spheroidal. These are well-known characteristics of connective tissues *in vivo* (53). The observations strongly demonstrate efficacy of magnetic assembly as a means to engineer tissues for basic studies as well as regenerative medicine.

Materials and Methods

Synthesis of magnetic nanoparticles

Magnetite (Fe_3O_4) nanoparticles were synthesized by a modification of Massart's co-precipitation method (54) and coated with bovine serum albumin (BSA) essentially as previously described (28). Briefly, 1.72 g $FeCl_2{\cdot}4H_2O$ and 4.67 g $FeCl_3{\cdot}6H_2O$ were dissolved in 60 ml deionized (DI) water. In order to ensure that the magnetite was not contaminated with maghemite (γ-Fe_2O_3) and hematite (α-Fe_2O_3) by oxygen dissolved in the reaction medium (55,56), the DI water was degassed prior to synthesis by boiling for ~30 min under vacuum and subsequent probe sonication for ~30 min. The solution was then added to 20 ml ammonium hydroxide with vigorous stirring. A black-brown precipitate of magnetite nanoparticles was formed. The mixture was centrifuged (5000 ***g***, 15 min) and the pellet resuspended in DI water to remove unreacted reagents and to reduce its pH. This process was repeated 5 times. MNPs were finally pelleted again and resuspended in 20 ml of 5% (w/v) aqueous solution of BSA (Fisher BioReagents, Pittsburgh, PA, USA. Fraction V, heat shock treated). The dispersion was sonicated for 1 h using a probe sonicator (Sonic Dismembrator; Model 300, Fisher Scientific, Pittsburgh, PA, USA). The resulting suspension was a homogeneous reddish brown liquid when inspected at 400× magnification using an inverted microscope. The solution was allowed to stand overnight, and then ultracentrifuged (Optima™ L-90K; Beckman-Coulter, Indianapolis, IN, USA) at 100 000 ***g*** for 1 h. The pellet was then resuspended in 40 ml DI water by sonication. This process removed excess BSA. The dispersion remained stable for several months when stored at 4 °C and contained a magnetite concentration of 50 mg/ml.

Cell culture

Human prostate cancer epithelial (PC-3) cells were obtained from American Type Culture Collection (ATCC) and cultured in Roswell Park Memorial Institute (RPMI) medium (Life Technologies, Carlsbad, CA, USA). The cells were transfected to express mOrange (PC3-mOrange) using full-length cDNA expressing mOrange, received as a kind gift from Dr. R. Y. Tsien, University of California, San Diego. *mOrange* gene was excised and cloned into pCDNA 3.1 and designated pCDNA-mOrange. PC3-mOrange cells were developed by following the stable transfection protocol as previ-

ously described (57). Briefly, the PC-3 cells were transfected with pCDNA-mOrange plasmid and grown under Geneticin restriction (2.5 μg/ml) for 2 weeks followed by selection of geneticin resistant clones under limiting dilution and further amplification. PC3-mOrange cells expressed mOrange stably for more than 50 passages in our laboratory. Human lung fibroblast (HFL-1) cells (ATCC) were cultured in Ham's F-12K (Kaighn's) medium (Life Technologies). All media were supplemented with heat inactivated 10% (v/v) foetal bovine serum (FBS; Atlanta Biologicals, Flowery Branch, GA, USA) and 1% (v/v) penicillin/streptomycin (Sigma-Aldrich, St. Louis, MO, USA). Additionally, the RPMI medium was supplemented with 1% (v/v) Geneticin (G418; Life Technologies) to select stably transfected PC3-mOrange cells. Cells were trypsinized and reseeded every 3–4 days then cultured at 37 °C in a humidified environment with 5% CO_2. The PC-3 cells used in the study were between their 20th and 40th passages, and HFL-1 cells were between 5th and 10th passages.

Cell magnetization

The dispersion of BSA coated MNPs in deionized water, prepared as described above, was diluted in Dulbecco's phosphate buffered saline at a ratio of 1:3 (v/v). This dilution had magnetite concentration of 12.5 mg/ml. The dilution factor was selected by trial-and-error; it produced distinctly observable magnetophoretic motion in almost all cells without significantly compromising their viability (discussed below). Cells were seeded in 12 well tissue culture plates (Nunc, Thermo Fisher Scientific, Waltham, MA, USA) at ~75% confluence and allowed to attach overnight. Each well was then washed and treated with the diluted MNP dispersion and incubated at 37 °C in a humidified environment with 5% CO_2 for 1 h. Cells were subsequently washed 5 times, trypsinized using standard techniques and used for the experiments. Cell viability was measured using trypan blue staining for dead cells and subsequent counting using a Nexcelom Cellometer (Nexcelom Bioscience, Lawrence, MA, USA).

Cluster formation using magnetic forces

Magnetized cells were assembled into 3D clusters on substrates using permanent magnets, as illustrated in Fig. 1. Cell clusters were built in layers using a multi-step seeding process (Fig. 1a). Briefly, a small droplet (~100 μl) of medium containing suspended magnetized cells was first placed on a glass coverslip immediately above the permanent magnets. The cells settled on the substrate within ~5 min due to magnetophoresis, forming a thin sheet whose shape was dictated by the magnetic field. Within an hour, these cells adhered to the glass substrate or to adjoining cells. A second drop of magnetized cell suspension was then dropped on top of the first. The process was repeated six times at 1 h intervals. An hour after the final seeding stage, the Petri dishes containing coverslips and magnets were filled with growth medium so that the coverslips and cells were completely submerged. After 24 h, the magnets were removed, the coverslips were immersed in growth medium and the cells were allowed to proliferate until the experiment was terminated by fixing the samples for microscopy.

Scanning electron microscopy

Scanning electron microscopy (SEM) images of the cells at various time points after seeding were obtained from samples fixed at the corresponding times. Karnovsky's fixative was prepared by dissolving 4 g paraformaldehyde powder in 50 ml distilled water at 70 °C. The solution cleared when a drop of potassium hydroxide was added. The solution was then cooled, 10 ml 50% glutaraldehyde was added, and the volume was brought up to 100 ml using 0.2 M sodium cacodylate. Finally, 50 mg calcium chloride was added slowly. 3D cell clusters, seeded on the glass coverslips, were first washed three times in PBS, then treated with Karnovsky's fixative and left at 4 °C overnight. Samples were subsequently washed in 0.1 M sodium cacodylate buffer for 15 min, post-fixed in 1% OsO_4 in 0.1 M sodium cacodylate buffer for 1 h, washed twice in sodium cacodylate buffer and dehydrated in series of graded ethanols. Then, the samples were dried (Ladd critical point dryer), coated with gold (SPI Module™ Sputter Coater) and imaged using a Carl Zeiss (Oberkochen, Germany) EVO 40 series SEM.

Confocal microscopy

The PC-3 cells were stably transfected to express mOrange and cultured in media supplemented with Geneticin as described above. Z-stack images of live 3D cell clusters were obtained using a Zeiss LSM510 META laser scanning microscope on an inverted Axio Observer Z1 base.

Results

Characterization of the magnetic nanoparticles

Size of the as-prepared BSA coated MNPs dispersed in DI water was measured using a variety of techniques. Their magnetic cores had diameters of ~10 nm, measured using transmission electron microscopy (Model: EM 420, Philips, Eindhoven, The Netherlands) (Fig. 2a,b). Hydrodynamic diameters of the particles, measured using

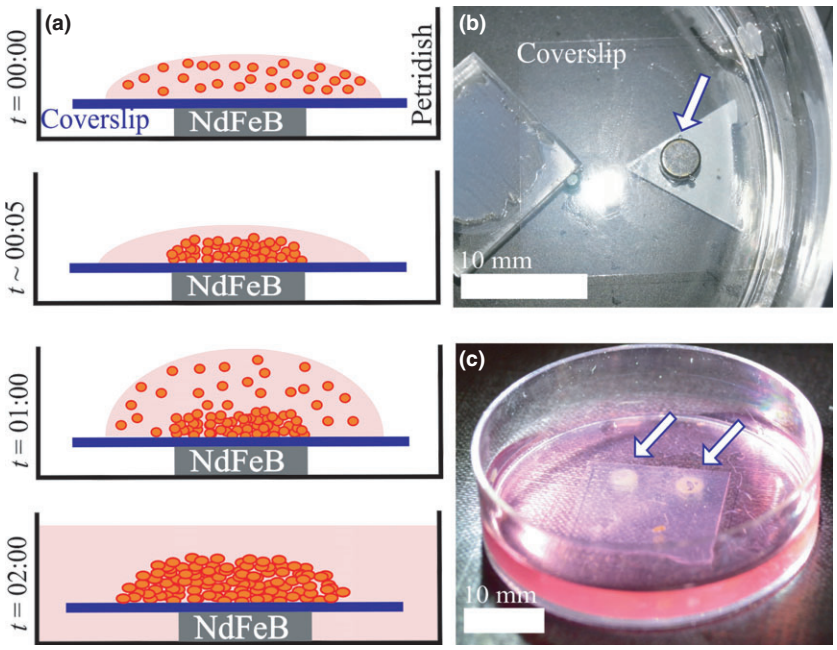

Figure 1. Magnetic assembly of 3D cell clusters. (a) Multi-step seeding process, where a thick 3D cluster of cells is built layer-wise by adding layers of cells at ~1 h intervals. (b) Configuration of the apparatus showing the coverslip over an NdFeB disc magnet (arrow). (c) Six seeding steps lead to a thick layer of cells that is visible to the naked eye (arrows).

Dynamic Light Scattering (Model: Zetasizer Nano ZS90, Malvern Instruments, Worcestershire, UK) had a modal value of ~50 nm (Fig. 2c). The difference occurred due to the thickness of protein coating as well as some agglomeration. Hydrodynamic diameters increased to ~80 nm when this dispersion was diluted in PBS prior to cell treatment, possibly due to further agglomeration.

Crystal structure of MNP cores was probed by X-ray powder diffraction (XRD) analysis (Bruker D8 Discover Davinci™ diffractometer, Co-Kα radiation: λ = 1.79 A) and patterns (Fig. 2d) showed characteristic peaks of Fe_3O_4 (PDF# 01-071-6336). Absence of weakly magnetic iron oxide α-Fe_2O_3 was confirmed since its characteristic peaks (PDF# 01-088-2359) were not observed. However, XRD analysis did not overrule the possibility of γ-Fe_2O_3 formation. This is because Fe_3O_4 and γ-Fe_2O_3 have almost identical crystal structures, making it impossible to distinguish between them using XRD (56).

Magnetization of MNPs was probed by recording their magnetic hysteresis (Fig. 2e) using a superconducting quantum interference device (SQUID) magnetometer (Magnetic Property Measurement System, Quantum Design Inc., San Diego, CA, USA). They did not show any observable remanence, that is, they were superparamagnetic. Further, room temperature saturation magnetization of MNPs matched that of Fe_3O_4 nanoparticles (~80 emu/g) (58,59) and were substantially higher than values reported for γ-Fe_2O_3 nanoparticles (~40 emu/g) (60,61). This confirmed that magnetic cores of the MNPs largely comprised of Fe_3O_4.

Variations in MNP concentration used in magnetizing the cells yielded variations in cell viability (Fig. 2f). Magnetite concentration of 12.5 mg/ml was the minimum that produced distinctly observable magnetophoretic motion in all cells. At this concentration, the whole magnetization process yielded PC-3 cell viability of 75.2 ± 5.6% (N = 4).

Cell morphology

Scanning electron microscopy was used to compare morphology of cells cultured as monolayers with those cultured in the magnetically assembled 3D clusters. In the monolayers, the familiar flattened morphology was assumed by both the PC-3 and HFL-1 cell lines (Fig. 3a,c). In contrast, in 3D clusters, both cell lines were visibly less stretched and assumed a somewhat spheroidal morphology (Fig. 3b,d).

Confocal microscopy (Fig. 4) was used to visualize morphology of PC-3 cells at various locations within 3D clusters. Cells that were in direct contact with the glass substrate had the familiar elongated form as observed in monolayers. In contrast, cells that were only in contact with other cells acquired spherical morphology.

Intercellular contacts

PC-3 cells in both monolayers (Fig. 3a) and 3D clusters (Fig. 3b) had extracellular fibers on their membrane surfaces. For cells in monolayers, these fibers did not serve

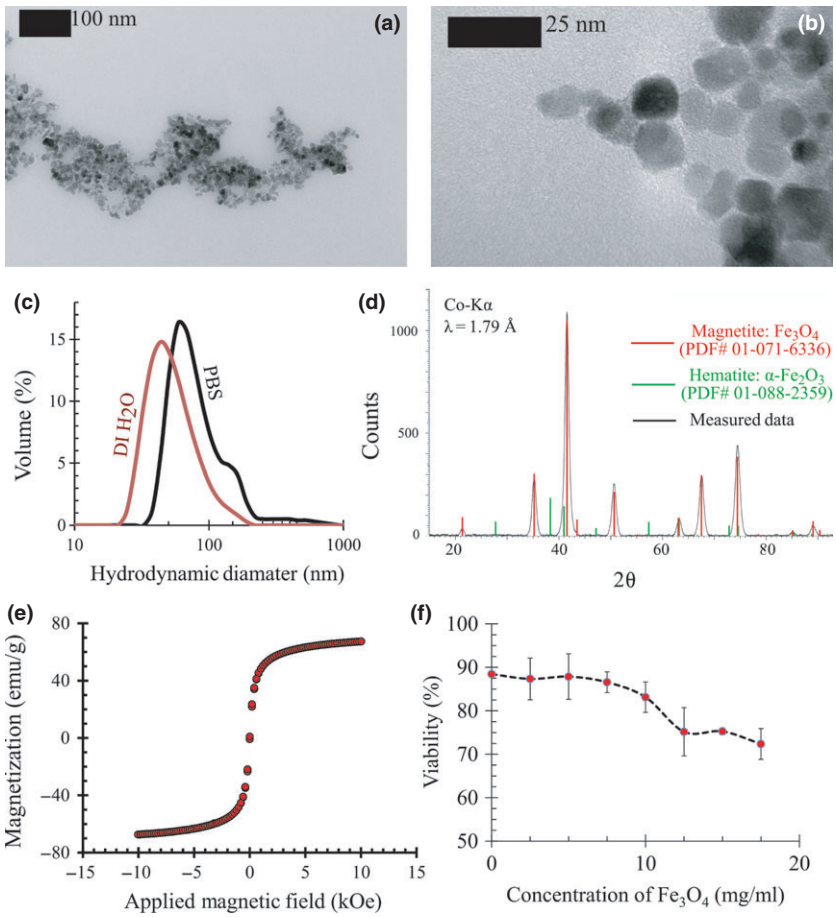

Figure 2. Characterization of the BSA coated MNPs. (a and b) TEM images show that the magnetite core of the MNPs has a diameter of ~10 nm. (c) Dynamic light scattering analysis shows that the modal value of the hydrodynamic diameter of BSA coated MNPs are ~50 nm in its original dispersion in DI water, and ~80 nm when the solution is diluted in PBS. (d) XRD pattern obtained from the nanoparticles shows all the peaks expected for the strongly magnetic iron oxide, magnetite (Fe_3O_4). Characteristic peaks of the weakly magnetic oxide, i.e., hematite (α-Fe_2O_3), are absent. (e) SQUID magnetometry shows that the saturation magnetization of the MNPs is ~80 emu/g, comparable with Fe_3O_4 nanoparticles. (f) Cytotoxicity of the magnetization process is evaluated by measuring the % viability of PC-3 cells at various concentrations of MNPs in PBS. Height of error bars = 2σ, $N = 4$.

any visible mechanical purpose (Fig. 3a). However, for those cultured in 3D clusters, the fibers formed intercellular contacts (Fig. 3b). HFL-1 cells in monolayers had smooth membranes (Fig. 3c) with no indication of the presence of extracellular fibers. However, in 3D clusters they had more surface asperities. These cells also formed large numbers of cell-cell contacts, aided by extracellular fibers (Fig. 3d).

Evolution of cluster shape

PC-3 cells were assembled into rings on Day 0 (Fig. 5a), after which they gradually organized themselves into tight circular sheets within a day. In some cells, cell membranes appeared stretched at points where they were attached to the intercellular fibers (Fig. 5b). This indicated that the fibers were in tension (62–65).

Temporal evolution of the shapes of cell clusters was even more dramatic for HFL-1 cells (Fig. 6). Starting from ring-like clusters visually indistinguishable from the Day 0 PC-3 cells (Fig. 5a), HFL-1 cells organized themselves into tightly packed spheroids within a day (Fig. 6a). Spheroidal clusters had much smaller diameters than initial rings.

Heterogeneities in cell morphology

Basolateral surfaces of HFL-1 clusters, detached from glass substrates, were formed of spheroidal cells with several cell-cell connections (Fig. 6b). Extracellular fibers aided such connections, as also seen in Fig. 3d. Cluster apical surfaces, on the other hand, were composed of smooth and stretched cells (Fig. 6c). These stretched cells were connected to each other at their boundaries by cytoplasmic protrusions that appeared like filopodia (Fig. 6d). The stretched cells formed a skin-like boundary over the entire spheroid surface that was exposed to culture media during growth.

Discussion

This study has examined contactless magnetic assembly of cells into 3D clusters as a scaffoldless means for generating *in vitro* tissue models. Unlike previous investigations, which used expression levels of generic proteins as a metric of efficacy (16,17,51,52), this study uses universal indicators of tissue formation: intercellular interactions and morphological features.

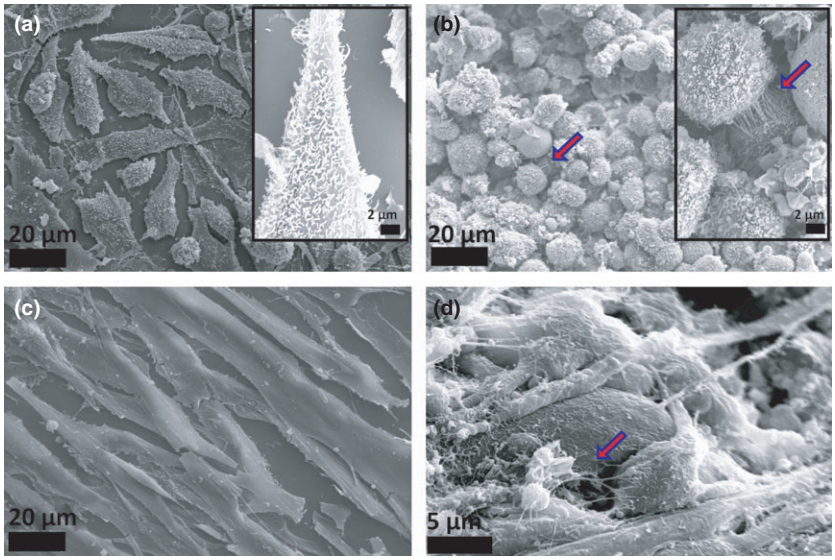

Figure 3. Cell morphology and intercellular contacts in magnetically assembled 3D clusters. (a) Human prostate cancer epithelial (PC-3) cells cultured in a monolayer on glass show the standard flattened morphology. Extracellular fibers (inset) are observed on their surface, but they do not form any inter-cellular connections. (b) When the same PC-3 cells are assembled into 3D clusters using magnetic forces, they assume a spherical shape and the fibers (inset) form inter-cellular connections (arrow). (c) Monolayers of human lung fibroblast (HFL-1) assume the flattened form, have smooth surfaces and do not show any extracellular fibers connecting neighboring cells. (d) HFL-1 cells assembled into 3D clusters are spheroidal and show multiple inter-cellular contacts aided by extra-cellular fibers (arrow).

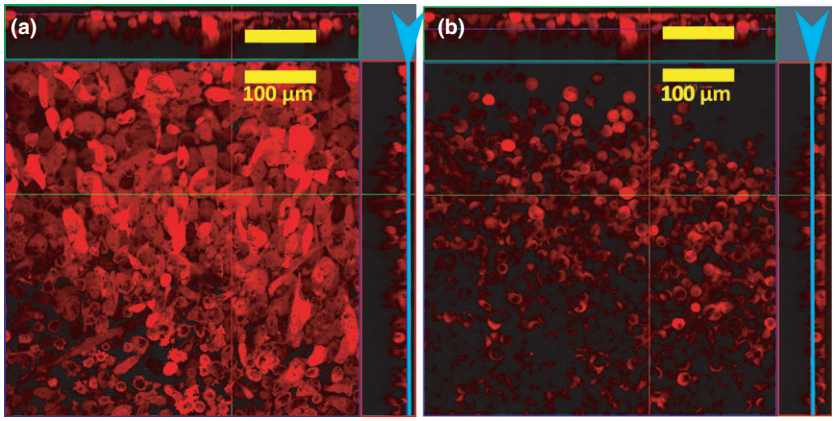

Figure 4. Z-stack analysis of a 3D culture of PC3-mOrange cells assembled by magnetic forces. (a) Cells on the lower end of the cluster that were in contact with the glass substrate of the coverslip show the familiar elongated form of monolayer culture, while (b) cells which have physical contact only with other cells acquired a spherical morphology. The light blue arrowhead and the line indicates the position in the Z-plane for the X-Y image shown.

Results demonstrate that despite the absence of artificial scaffolding materials, the cells collectively organized to present visible features of an *in vivo* tissue.

Cell morphology in 3D clusters differed substantially from monolayers

Cell morphology strongly depends on the mechanical stiffness of the material in contact with it (66–69). Thus, for accurate modeling of *in vivo* tissues, cell culture methods must mimic the stiffness of the *in vivo* cellular microenvironment, which is comprised of neighboring cells and the ECM. Scaffolds used in conventional 3D cell culture methods are foreign to the cells, thus they differ in stiffness from the natural cellular microenvironment. Instead, magnetic assembly delivers a closer approximation. The cultured cells are initially only in contact with other neighboring cells, and thereafter also with the extracellular materials that they produce. This has a profound impact on cell morphology when compared to monolayers (Fig. 3). The cells assume a spheroidal shapes as opposed to the familiar flattened form observed in monolayers and certain artificial scaffolds (9,10). Even within a 3D cluster, cells in direct contact with the stiff glass substrate have flattened monolayer shapes, while those which only contact other cells acquire spherical morphology (Fig. 4). This confirms the need for mimicking mechanical stiffness of the cellular microenvironment for accurate representation of a tissue in an *in vitro* model.

Cell-cell connections serve the mechanical function of scaffolds

When a fresh single cell suspension is seeded for culture, cell-cell contacts are non-existent or extremely weak, and thus unable to bear the weight of the cells.

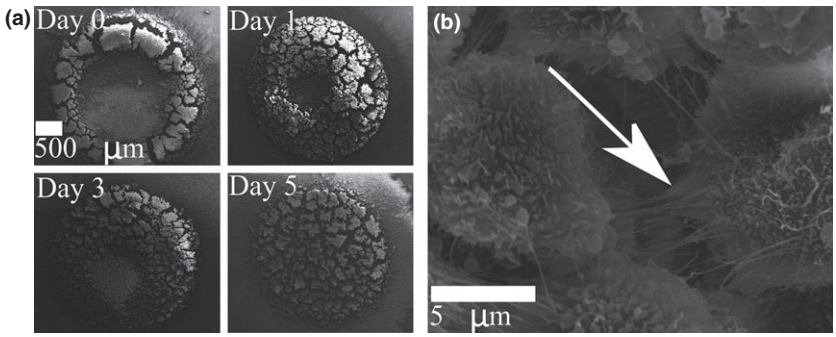

Figure 5. Human prostate cancer epithelial (PC-3) cells self-organize into a multilayer sheet. (a) PC-3 cells were initially assembled into a ring under magnetic force. The cells self-organized into a multilayered circular sheet within a day. (b) Evidence of tension on an intercellular fiber given by the stretching observed in the membrane of the attached cell (arrow) suggests that the fibers enabled the self-organization.

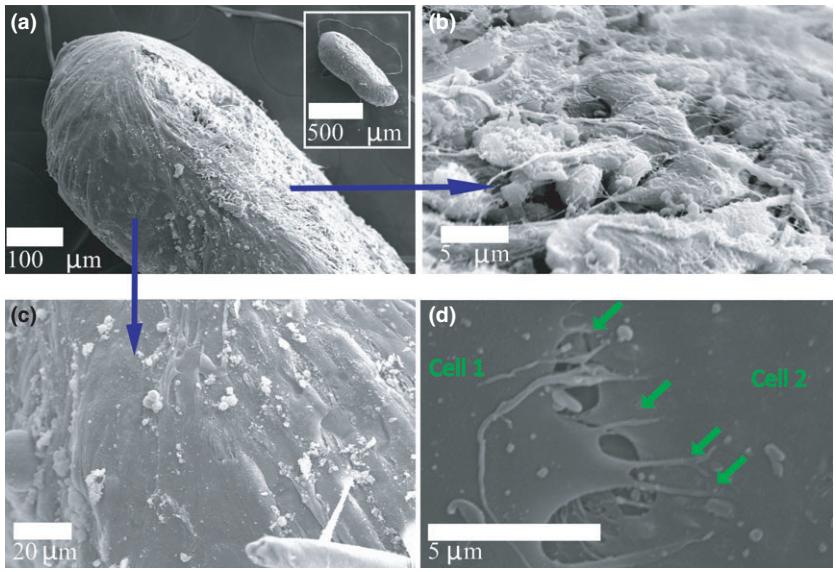

Figure 6. Human lung fibroblast (HFL-1) cells self-organized into a tight spheroid. (a) Side view of a 3D cluster (inset: lower magnification) shows the flattened-spheroid shape assumed by the HFL-1 cells. (b) The basolateral surface of the cluster that was in contact with the glass coverslip contained cells with a rounded morphology. Several inter-cellular contacts aided by extra-cellular fibers are seen. (c) The apical surface, which formed the interface between the cluster and the culture medium, was smooth and comprised of skin-like stretched cells. (d) The stretched cells formed inter-cellular contacts through filopodia-like protrusions (arrows).

As a result, cells settle on culture substrates under gravity, forming the well-known monolayer culture. Its architecture is quite different from an *in vivo* tissue, and this difference is known to influence cell function. To better mimic a tissue, conventional 3D cell culture methods use scaffolds to position cells in a 3D architecture, thereby implementing the cell-cell proximity encountered *in vivo* (69,70). The scaffold is merely a 3D frame that mechanically supports cells by direct physical contact. Instead, in this study, magnetic forces have been used to provide mechanical support. We observed that once cells were thus supported for ~1 day, they naturally adhered to each other and retained their 3D structure even when the magnetic forces were removed. For the PC-3 and HFL-1 cells examined, the adherence resulted from cell-cell connections formed using extracellular fibers (Fig. 3), which developed sufficient strength to support weight of the cells within the day. Thus, the primary function of scaffolds was served by the magnetic forces and thereafter by the cell-cell interconnections. This eliminated the need for physical contact with artificial scaffold material.

Clusters evolved to resemble corresponding tissues in vivo

A tissue culture method is successful if the cultured cells self-organize to resemble their corresponding *in vivo* tissue. This is rarely observed in monolayers. However, here both cell types self-organized into structures resembling their corresponding tissues *in vivo*: the epithelial cells (PC-3) formed multi-layer sheets (Fig. 5), while the fibroblasts (HFL-1) formed tightly packed spheroids (Fig. 6). We believe that the close cell-cell proximity facilitated by magnetic assembly enabled inter-cellular microenvironmental cues that yielded such organization. Intercellular fibers were seen to apply forces to the cells (Fig. 5b), and possibly aid in this self-organization. Measurement of such forces, particularly their evolution with tissue morphology, will provide significant advances to our understanding of tissue morphogenesis. This can be accomplished using well-calibrated matrices (71) or by comparison with magnetostatic forces (26).

3D spheroids of HFL-1 cells (Fig. 6) demonstrated a very interesting feature: cells on the peripheries of 3D

clusters adopted different morphologies from cells contained within. This demonstrates that assembled cells readily differentiated their morphology based on cues from their environment. Such position-dependent morphological differentiation is well known in connective tissues *in vivo* (53). They often serve crucial functions of the corresponding tissue.

Adoption of magnetic assembly for organotypic cell culture

Observations in this study provide evidence of the efficacy of magnetic assembly in tissue engineering by demonstrating that, despite the absence of artificial scaffolding materials, cells can organize themselves towards a functional form through intercellular contacts after accepting mechanical and micro environmental cues. The method described can be readily adopted in any laboratory practicing cell culture. It can be used to generate 3D clusters comprising single cell types or many different cell types, as seen in tissue architecture *in vivo*. Thus, the method has enormous and wide-ranging scope for functional studies of various cell types.

Fairly exhaustive reports, for example, cytotoxicity and quantity of uptake, of similarly prepared MNPs on a wide variety of cell types are available in the literature. A list of common cell types is presented below, sorted by the coating material used on the MNPs.

1 *BSA coated MNPs* have been used to magnetize mouse embryonic fibroblasts (MEF), rat placental cells (GH3), human cervical cells (HeLa), breast cells (MCF-7) and liver (HepG2) cancer cells (28,72) as well as the cell lines studied here, human prostate cancer (PC-3) and lung fibroblasts (HFL-1).
2 *Magnetic cationic liposomes*, comprising MNPs coated in lipid molecules, have been used to magnetize primary cells, such as neonatal foreskin keratinocytes, umbilical vein endothelium (HUVEC), dermal fibroblasts, aortic endothelial and smooth muscle cells, immortalized cell lines such as human retinal pigment epithelium (ARPE-19), mouse fibroblasts (NIH 3T3) and myoblasts (C2C12), stem cells such as human bone marrow mesenchymal stem cells (MSCs), mouse hepatocytes and canine urothelial cells (33–38,40,73–75).
3 *Hydrogels, comprising of gold, filamentous bacteriophages and MNPs* have been used to label human astrocytes, glioblastoma cells (LN-229 and U-251MG), pulmonary microvascular endothelium (PEC), bronchial epithelium (EpiC), pulmonary fibroblasts, tracheal smooth muscle and lung epithelial (A549) cells, and mouse preadipocytes (3T3-L1), brain endothelium (bEND.3) and neural stem (C17.2) cells (17,51,52,76). The method described has been commercialized by n3D Biosciences Inc. of Houston, TX, USA.
4 *Pullulan coated MNPs* have been used to magnetize telomerase-immortalized primary human fibroblasts (hTERT-BJ1) (77).
5 *Dextran and silan coated MNPs* have been used to magnetize human cerebral cortical neuronal (HCN-2), mammary carcinoma (BT20) and colonic adenocarcinoma (WiDr) cell lines, primary fibroblasts obtained by punch biopsy and primary cells derived from a glioblastoma multiformae patient (78).
6 *Silica coated MNPs* have been used to magnetize mouse endothelial yolk-sac (C166) cells (32).
7 *Folic acid coated MNPs* have been used to selectively magnetize folate overexpressing cancer cells, such as mouse melanoma (B16-F0) and human cervical cancer (HeLa) cells (30).

While materials coating MNPs diminish their cytotoxicity and ensure rapid internalization, long term effects of MNPs are not yet fully established. This is a pertinent question when considering magnetic assembly as a means to develop tissues for implantation. As yet few studies have focused on long term effects in mice (79,80) and these show that dextran coated MNPs, known to be internalized into cells initially (81), are thereafter retained as clusters in the liver and spleen. However, magnetite retention did not produce any morphological alterations or cell damage in the respective organs. Further, after about 3 months, iron was seen to be released from the MNPs, which may indicate elimination by reabsorption.

Acknowledgements

We thank Kathy Lowe of the Virginia-Maryland Regional College of Veterinary Medicine for sample preparation and user training for SEM imaging, Kristi DeCourcy of the Fralin Life Science Institute at Virginia Tech for assistance with confocal imaging, Chris Winkler and the ICTAS Nanoscale Characterization and Fabrication Facility at Virginia Tech for TEM imaging of nanoparticles, Sonal Mazumdar, Sharavanan Balasubramanian and Richey Davis for access to and user training of DLS, Daniel Dudek for the use of fume hood in nanoparticle synthesis, Victoria Jarvis of the McMaster Analytical X-Ray Diffraction Facility and Ahmed M Abdalla of the Department of Engineering Physics, McMaster University for XRD Analysis, Paul Dube of the Brockhouse Institute for Materials Research at McMaster University for SQUID magnetometry and Moanaro Biswas for helpful discussions. Part of this work was supported by a Natural Sciences

and Engineering Research Council of Canada Discovery Grant.

References

1 Pampaloni F, Reynaud EG, Stelzer EHK (2007) The third dimension bridges the gap between cell culture and live tissue. *Nat. Rev. Mol. Cell Biol.* **8**, 839–845.
2 Rimann M, Graf-Hausner U (2012) Synthetic 3D multicellular systems for drug development. *Curr. Opin. Biotechnol.* **23**, 803–809.
3 Kelm JM, Lorber V, Snedeker JG, Schmidt D, Broggini-Tenzer A, Weisstanner M *et al.* (2010) A novel concept for scaffold-free vessel tissue engineering: self-assembly of microtissue building blocks. *J. Biotechnol.* **148**, 46–55.
4 Tung Y-C, Hsiao AY, Allen SG, Torisawa Y-S, Ho M, Takayama S (2011) High-throughput 3D spheroid culture and drug testing using a 384 hanging drop array. *Analyst* **136**, 473–478.
5 Bergthorsson JT, Magnusson MK, Gudjonsson T (2012) Endothelial-rich microenvironment supports growth and branching morphogenesis of prostate epithelial cells. *The Prostate* **73**, 884–896.
6 Engler AJ, Sen S, Sweeney HL, Discher DE (2006) Matrix elasticity directs stem cell lineage specification. *Cell* **126**, 677–689.
7 Lutolf MP, Hubbell JA (2005) Synthetic biomaterials as instructive extracellular microenvironments for morphogenesis in tissue engineering. *Nat. Biotech.* **23**, 47–55.
8 Zorlutuna P, Annabi N, Camci-Unal G, Nikkhah M, Cha JM, Nichol JW *et al.* (2012) Microfabricated biomaterials for engineering 3D tissues. *Adv. Mater.* **24**, 1782–1804.
9 Teo BKK, Goh KJ, Ng ZJ, Koo S, Yim EKF (2012) Functional reconstruction of corneal endothelium using nanotopography for tissue-engineering applications. *Acta Biomater.* **8**, 2941–2952.
10 Yim EKF, Darling EM, Kulangara K, Guilak F, Leong KW (2010) Nanotopography-induced changes in focal adhesions, cytoskeletal organization, and mechanical properties of human mesenchymal stem cells. *Biomaterials* **31**, 1299–1306.
11 Hughes CS, Postovit LM, Lajoie GA (2010) Matrigel: a complex protein mixture required for optimal growth of cell culture. *Proteomics* **10**, 1886–1890.
12 Blow N (2009) Cell culture: building a better matrix. *Nat. Meth.* **6**, 619–622.
13 Vukicevic S, Kleinman HK, Luyten FP, Roberts AB, Roche NS, Reddi A (1992) Identification of multiple active growth factors in basement membrane Matrigel suggests caution in interpretation of cellular activity related to extracellular matrix components. *Exp. Cell Res.* **202**, 1–8.
14 Fischbach C, Chen R, Matsumoto T, Schmelzle T, Brugge JS, Polverini PJ *et al.* (2007) Engineering tumors with 3D scaffolds. *Nat. Methods* **4**, 855–860.
15 Johnstone B, Hering TM, Caplan AI, Goldberg VM, Yoo JU (1998) In vitro chondrogenesis of bone marrow-derived mesenchymal progenitor cells. *Exp. Cell Res.* **238**, 265–272.
16 Fayol D, Frasca G, Le Visage C, Gazeau F, Luciani N, Wilhelm C (2013) Use of magnetic forces to promote stem cell aggregation during differentiation, and cartilage tissue modeling. *Adv. Mater.* **25**, 2611–2616.
17 Souza GR, Molina JR, Raphael RM, Ozawa MG, Stark DJ, Levin CS *et al.* (2010) Three-dimensional tissue culture based on magnetic cell levitation. *Nat. Nano.* **5**, 291–296.
18 Kelm JM, Timmins NE, Brown CJ, Fussenegger M, Nielsen LK (2003) Method for generation of homogeneous multicellular tumor spheroids applicable to a wide variety of cell types. *Biotechnol. Bioeng.* **83**, 173–180.
19 Owen CS, Sykes NL (1984) Magnetic labeling and cell sorting. *J. Immunol. Methods* **73**, 41–48.
20 Pankhurst QA, Connolly J, Jones SK, Dobson J (2003) Applications of magnetic nanoparticles in biomedicine. *J. Phys. D Appl. Phys.* **36**, R167.
21 Pankhurst QA, Thanh NKT, Jones SK, Dobson J (2009) Progress in applications of magnetic nanoparticles in biomedicine. *J. Phys. D Appl. Phys.* **42**, 224001.
22 Clavijo-Jordan V, Kodibagkar VD, Beeman SC, Hann BD, Bennett KM (2012) Principles and emerging applications of nanomagnetic materials in medicine. *Wiley Interdiscip. Rev. Nanomed. Nanobiotechnol.* **4**, 345–365.
23 Kose AR, Fischer B, Mao L, Koser H (2009) Label-free cellular manipulation and sorting via biocompatible ferrofluids. *Proc. Natl Acad. Sci.* **106**, 21478–21483.
24 Ino K, Ito A, Honda H (2007) Cell patterning using magnetite nanoparticles and magnetic force. *Biotechnol. Bioeng.* **97**, 1309–1317.
25 Krebs MD, Erb RM, Yellen BB, Samanta B, Bajaj A, Rotello VM *et al.* (2009) Formation of ordered cellular structures in suspension via label-free negative magnetophoresis. *Nano Lett.* **9**, 1812–1817.
26 Tseng P, Judy JW, Di Carlo D (2012) Magnetic nanoparticle-mediated massively parallel mechanical modulation of single-cell behavior. *Nat. Meth.* **9**, 1113–1119.
27 Frasca G, Du V, Bacri J-C, Gazeau F, Gay C, Wilhelm C (2014) Magnetically shaped cell aggregates: from granular to contractile materials. *Soft Matter.* **10**, 5045–5054.
28 Bajaj A, Samanta B, Yan H, Jerry DJ, Rotello VM (2009) Stability, toxicity and differential cellular uptake of protein passivated-Fe_3O_4 nanoparticles. *J. Mater. Chem.* **19**, 6328–6331.
29 Wilhelm C, Gazeau F (2008) Universal cell labelling with anionic magnetic nanoparticles. *Biomaterials* **29**, 3161–3174.
30 Mohapatra S, Mallick S, Maiti T, Ghosh S, Pramanik P (2007) Synthesis of highly stable folic acid conjugated magnetite nanoparticles for targeting cancer cells. *Nanotechnology* **18**, 385102.
31 Frasca G, Gazeau F, Wilhelm C (2009) Formation of a three-dimensional multicellular assembly using magnetic patterning. *Langmuir* **25**, 2348–2354.
32 Whatley BR, Li X, Zhang N, Wen X (2014) Magnetic-directed patterning of cell spheroids. *J. Biomed. Mater. Res. Part A* **102**, 1537–1547.
33 Fujita H, Shimizu K, Yamamoto Y, Ito A, Kamihira M, Nagamori E (2010) Fabrication of scaffold-free contractile skeletal muscle tissue using magnetite-incorporated myogenic C_2C1_2 cells. *J Tissue Eng. Regen. Med.* **4**, 437–443.
34 Yamamoto Y, Ito A, Fujita H, Nagamori E, Kawabe Y, Kamihira M (2011) Functional evaluation of artificial skeletal muscle tissue constructs fabricated by a magnetic force-based tissue engineering technique. *Tissue Eng. Part A* **17**, 107–114.
35 Ito A, Hayashida M, Honda H, Hata KI, Kagami H, Ueda M *et al.* (2004) Construction and harvest of multilayered keratinocyte sheets using magnetite nanoparticles and magnetic force. *Tissue Eng.* **10**, 873–880.
36 Ito A, Hibino E, Kobayashi C, Terasaki H, Kagami H, Ueda M *et al.* (2005) Construction and delivery of tissue-engineered human retinal pigment epithelial cell sheets, using magnetite nanoparticles and magnetic force. *Tissue Eng.* **11**, 489–496.
37 Ino K, Ito A, Kumazawa H, Kagami H, Ueda M, Honda H (2007) Incorporation of capillary-like structures into dermal cell sheets constructed by magnetic force-based tissue engineering. *J. Chem. Eng. Jpn.* **40**, 51–58.
38 Ito A, Ino K, Hayashida M, Kobayashi T, Matsunuma H, Kagami H *et al.* (2005) Novel methodology for fabrication of tissue-engi-

neered tubular constructs using magnetite nanoparticles and magnetic force. *Tissue Eng.* **11**, 1553–1561.
39 Perea H, Aigner J, Hopfner U, Wintermantel E (2006) Direct magnetic tubular cell seeding: a novel approach for vascular tissue engineering. *Cells Tissues Organs.* **183**, 156–165.
40 Shimizu K, Ito A, Yoshida T, Yamada Y, Ueda M, Honda H (2007) Bone tissue engineering with human mesenchymal stem cell sheets constructed using magnetite nanoparticles and magnetic force. *J. Biomed. Mater. Res. Part B* **82B**, 471–480.
41 Akiyama H, Ito A, Sato M, Kawabe Y, Kamihira M (2010) Construction of cardiac tissue rings using a magnetic tissue fabrication technique. *Int. J. Mol. Sci.* **11**, 2910–2920.
42 Ghosh S, Puri IK (2013) Soft polymer magnetic nanocomposites: microstructure patterning by magnetophoretic transport and self-assembly. *Soft Matter.* **9**, 2024–2029.
43 Ghosh S, Tehrani M, Al-Haik MS, Puri IK (2015) Patterning the stiffness of elastomeric nanocomposites by magnetophoretic control of cross-linking impeder distribution. *Materials* **8**, 474–485.
44 Henderson J, Shi S, Cakmaktepe S, Crawford TM (2012) Pattern transfer nanomanufacturing using magnetic recording for programmed nanoparticle assembly. *Nanotechnology* **23**, 185304.
45 Tracy JB, Crawford TM (2013) Magnetic field-directed self-assembly of magnetic nanoparticles. *MRS Bull.* **38**, 915–920.
46 Fragouli D, Buonsanti R, Bertoni G, Sangregorio C, Innocenti C, Falqui A *et al.* (2010) Dynamical formation of spatially localized arrays of aligned nanowires in plastic films with magnetic anisotropy. *ACS Nano* **4**, 1873–1878.
47 Ino K, Okochi M, Konishi N, Nakatochi M, Imai R, Shikida M *et al.* (2007) Cell culture arrays using magnetic force-based cell patterning for dynamic single cell analysis. *Lab. Chip.* **8**, 134–142.
48 Grivennikov S, Karin M (2008) Autocrine IL-6 signaling: a key event in tumorigenesis? *Cancer Cell* **13**, 7–9.
49 Ghosh S, Elankumaran S, Puri IK (2011) Mathematical model of the role of intercellular signalling in intercellular cooperation during tumorigenesis. *Cell Prolif.* **44**, 192–203.
50 Lee EA, Yim H, Heo J, Kim H, Jung G, Hwang NS (2014) Application of magnetic nanoparticle for controlled tissue assembly and tissue engineering. *Arch. Pharm. Res.* **37**, 120–128.
51 Tseng H, Gage JA, Raphael RM, Moore RH, Killian TC, Grande-Allen KJ *et al.* (2013) Assembly of a three-dimensional multitype bronchiole coculture model using magnetic levitation. *Tissue Eng. Part C Methods* **19**, 665–675.
52 Daquinag AC, Souza GR, Kolonin MG (2013) Adipose tissue engineering in three-dimensional levitation tissue culture system based on magnetic nanoparticles. *Tissue Eng. Part C Methods* **19**, 336–344.
53 Hakkinen L, Larjava H (1992) Characterization of fibroblast clones from periodontal granulation tissue in vitro. *J. Dent. Res.* **71**, 1901–1907.
54 Massart R (1981) Preparation of aqueous magnetic liquids in alkaline and acidic media. *IEEE T Magn.* **17**, 1247–1248.
55 Karaagac O, Kockar H, Beyaz S, Tanrisever T (2010) A simple way to synthesize superparamagnetic iron oxide nanoparticles in air atmosphere: iron ion concentration effect. *IEEE Trans. Magn.* **46**, 3978–3983.
56 Maity D, Agrawal D (2007) Synthesis of iron oxide nanoparticles under oxidizing environment and their stabilization in aqueous and non-aqueous media. *J. Magn. Magn. Mater.* **308**, 46–55.
57 Jang J, Hong SH, Choi D, Choi KS, Kang S, Kim IH (2010) Overexpression of Newcastle disease virus (NDV) V protein enhances NDV production kinetics in chicken embryo fibroblasts. *Appl. Microbiol. Biotechnol.* **85**, 1509–1520.
58 Daou T, Greneche J, Pourroy G, Buathong S, Derory A, Ulhaq-Bouillet C *et al.* (2008) Coupling agent effect on magnetic properties of functionalized magnetite-based nanoparticles. *Chem. Mater.* **20**, 5869–5875.
59 Mascolo M, Pei Y, Ring T (2013) Room temperature co-precipitation synthesis of magnetite nanoparticles in a large pH window with different bases. *Materials* **6**, 5549–5567.
60 Jeong J-R, Lee S-J, Kim J-D, Shin S-C (2004) Magnetic properties of g-Fe_2O_3 nanoparticles made by coprecipitation method. *Phys. Status Solidi B Basic Res.* **241**, 1593–1596.
61 Millan A, Urtizberea A, Silva N, Palacio F, Amaral V, Snoeck E *et al.* (2007) Surface effects in maghemite nanoparticles. *J. Magn. Magn. Mater.* **312**, L5–L9.
62 Legant WR, Choi CK, Miller JS, Shao L, Gao L, Betzig E *et al.* (2013) Multidimensional traction force microscopy reveals out-of-plane rotational moments about focal adhesions. *Proc. Natl Acad. Sci. U.S.A.* **110**, 881–886.
63 Ladoux B, Nicolas A (2012) Physically based principles of cell adhesion mechanosensitivity in tissues. *Rep. Prog. Phys.* **75**, 116601.
64 Koch TM, Münster S, Bonakdar N, Butler JP, Fabry B (2012) 3D traction forces in cancer cell invasion. *PLoS ONE* **7**, e33476.
65 Banerjee S, Marchetti MC (2013) Controlling cell–matrix traction forces by extracellular geometry. *New J. Phys.* **15**, 035015.
66 Subramanian A, Lin HY (2005) Crosslinked chitosan: its physical properties and the effects of matrix stiffness on chondrocyte cell morphology and proliferation. *J. Biomed. Mater. Res. Part A* **75**, 742–753.
67 Levy-Mishali M, Zoldan J, Levenberg S (2009) Effect of scaffold stiffness on myoblast differentiation. *Tissue Eng. Part A* **15**, 935–944.
68 Subramanian B, Rudym D, Cannizzaro C, Perrone R, Zhou J, Kaplan DL (2010) Tissue-engineered three-dimensional in vitro models for normal and diseased kidney. *Tissue Eng. Part A* **16**, 2821–2831.
69 Dado D, Levenberg S (2009) Cell–Scaffold Mechanical Interplay within Engineered Tissue. *Semin. Cell Dev. Biol*. **20**, 656–664.
70 Levenberg S, Langer R (2004) Advances in tissue engineering. *Curr. Top. Dev. Biol.* **61**, 113–134.
71 Legant WR, Miller JS, Blakely BL, Cohen DM, Genin GM, Chen CS (2010) Measurement of mechanical tractions exerted by cells in three-dimensional matrices. *Nat. Methods* **7**, 969–971.
72 Samanta B, Yan H, Fischer NO, Shi J, Jerry DJ, Rotello VM (2008) Protein-passivated Fe_3O_4 nanoparticles: low toxicity and rapid heating for thermal therapy. *J. Mater. Chem.* **18**, 1204–1208.
73 Ito A, Takizawa Y, Honda H, Hata KI, Kagami H, Ueda M *et al.* (2004) Tissue engineering using magnetite nanoparticles and magnetic force: heterotypic layers of cocultured hepatocytes and endothelial cells. *Tissue Eng.* **10**, 833–840.
74 Shimizu K, Ito A, Honda H (2006) Enhanced cell-seeding into 3D porous scaffolds by use of magnetite nanoparticles. *J. Biomed. Mater. Res. Part B* **77B**, 265–272.
75 Ito A, Hibino E, Honda H, K-i Hata, Kagami H, Ueda M *et al.* (2004) A new methodology of mesenchymal stem cell expansion using magnetic nanoparticles. *Biochem. Eng. J.* **20**, 119–125.
76 Haisler WL, Timm DM, Gage JA, Tseng H, Killian TC, Souza GR (2013) Three-dimensional cell culturing by magnetic levitation. *Nat. Protocols.* **8**, 1940–1949.
77 Gupta AK, Gupta M (2005) Cytotoxicity suppression and cellular uptake enhancement of surface modified magnetic nanoparticles. *Biomaterials* **26**, 1565–1573.

78 Jordan A, Scholz R, Wust P, Schirra H, Schiestel T, Schmidt H *et al.* (1999) Endocytosis of dextran and silan-coated magnetite nanoparticles and the effect of intracellular hyperthermia on human mammary carcinoma cells in vitro. *J. Magn. Magn. Mater.* **194**, 185–196.

79 Estevanato LL, Lacava LM, Carvalho LC, Azevedo RB, Silva O, Pelegrini F *et al.* (2012) Long-term biodistribution and biocompatibility investigation of dextran-coated magnetite nanoparticle using mice as the animal model. *J. Biomed. Nanotechnol.* **8**, 301–308.

80 Lacava L, Garcia V, Kückelhaus S, Azevedo R, Sadeghiani N, Buske N *et al.* (2004) Long-term retention of dextran-coated magnetite nanoparticles in the liver and spleen. *J. Magn. Magn. Mater.* **272**, 2434–2435.

81 Yu M, Huang S, Yu KJ, Clyne AM (2012) Dextran and polymer polyethylene glycol (PEG) coating reduce both 5 and 30 nm iron oxide nanoparticle cytotoxicity in 2D and 3D cell culture. *Int. J. Mol. Sci.* **13**, 5554–5570.